NAWCWPNS TP 8334

A Real-Space, Numerical-Integration Approach To Calculating Diffraction From Gratings

by
J. Merle Elson and Phuc Tran
Research & Technology Group

December 1996

NAVAL AIR WARFARE CENTER WEAPONS DIVISION
CHINA LAKE, CA 93555-6100

Approved for public release; distribution is unlimited.

Naval Air Warfare Center Weapons Division

FOREWORD

This work was supported in part by a grant of High Performance Computing (HPC) time from the DOD HPC Center, U. S. Army Corps of Engineers Waterways Experiment Station (Cray Research C-916 and Y-MP). The authors were supported by Navy In-House Independent Research Funds.

This report is a working document subject to change and was reviewed for technical accuracy by Fernando Escobar.

Approved by
R. L. Derr, *Head*
Research & Technology Group
25 November 1996

Under authority of
J. V. Chenevey
RADM, U.S. Navy
Commander

Released for publication by
S. HAALAND
Director for Research and Engineering

NAWCWPNS Technical Publication 8334

Published by . . . . . Technical Information Division
Collation . . . . . Cover, 5 leaves
First printing . . . . . 35 copies

REPORT DOCUMENTATION PAGE

Form Approved
OMB No. 0704-0188

1. AGENCY USE ONLY *(Leave blank)*	2. REPORT DATE	3. REPORT TYPE AND DATES COVERED
	December 1996	Interim report - October 1995-September 1996

4. TITLE AND SUBTITLE
A Real-Space, Numerical-Integration Approach To Calculating Diffraction From Gratings

5. FUNDING NUMBERS
N0001496WX20167

6. AUTHOR(S)
J. Merle Elson and Phuc Tran

7. PERFORMING ORGANIZATION NAME(S) AND ADDRESS(ES)
Naval Air Warfare Center Weapons Division
China Lake, CA 93555-6100

8. PERFORMING ORGANIZATION REPORT NUMBER
NAWCWPNS TP 8334

9. SPONSORING/MONITORING AGENCY NAME(S) AND ADDRESS(ES)
Office of Naval Research
ONR 354-Dr. Ronald Kostoff
Ballston Tower One
800 N. Quincy St.
Arlington, VA 22217-5660

10. SPONSORING/MONITORING AGENCY REPORT NUMBER

11. SUPPLEMENTARY NOTES

12A. DISTRIBUTION/AVAILABILITY STATEMENT
A Statement; distribution unlimited

12B. DISTRIBUTION CODE

13. ABSTRACT *(Maximum 200 words)*

(U) We write Maxwell's equations in finite difference form and, along with the **R**-matrix propagation algorithm, numerically integrate to obtain solutions for grating diffraction. Numerical results are obtained for a sinusoidal grating and are compared with previous results obtained from other methods.

14. SUBJECT TERMS
Diffraction
R-Matrix
Grating
Electromagnetic Theory
Finite Difference

15. NUMBER OF PAGES
9

16. PRICE CODE

17. SECURITY CLASSIFICATION OF REPORT	18. SECURITY CLASSIFICATION OF THIS PAGE	19. SECURITY CLASSIFICATION OF ABSTRACT	20. LIMITATION OF ABSTRACT
UNCLASSIFIED	UNCLASSIFIED	UNCLASSIFIED	UL

INTRODUCTION

In this report, we briefly describe the method used and numerical results obtained for diffraction from an absorbing gold metallic grating with a sinusoidal profile having period $d = 2\lambda$ and $h = 0.4\lambda$, where h is the peak-to-valley grating height and λ is the wavelength. This grating has been previously discussed by Depine (Reference 1), and we compare our results below with prior results presented in that paper. We have previously compared our results with Depine, as described in Elson and Tran (Reference 2), where an approach that has similarities to that presented here was used. Further, in this work we will also compare the Depine results with yet another method previously described by Elson and Tran (Reference 3) where this approach was also used to investigate surface wave dispersion on truncated photonic crystals (Reference 4). Finally, the method used in this work is identical to that given by Elson and Tran (Reference 5), which was previously used to calculate bulk dispersion of photonic media and transmission of finite thickness photonic media.

Depine used a surface impedance boundary condition method. Elson and Tran (Reference 2) used a modal expansion method where Maxwell's equations were partially written in Fourier space and the resulting differential equations were solved as eigenfunction expansions. The approaches shown in References 3 and 4 are very similar to Reference 2 except that Maxwell's equations are approximated by finite difference equations and the solutions are obtained entirely in real-space.

As also shown in Reference 5, the approach used in this work writes Maxwell's equations entirely in finite difference form and then numerically integrates through the profile region to obtain the solution. As in References 2 through 5, the **R**-matrix propagation algorithm is used because of inherent numerical stability. The calculation method is outlined below.

CALCULATION OUTLINE

We consider a sinusoidal grating, shown in Figure 1, which is invariant in the $\hat{\mathbf{y}}$ direction and periodic in the $\hat{\mathbf{x}}$ direction. The profile shape is $z = f(x)$ and is confined to a finite thickness region in the $\hat{\mathbf{z}}$ direction. The semi-infinite substrate and superstrate are homogeneous and the finite thickness region in between, which contains the grating profile, is described by a spatially variable permittivity $\varepsilon(x,z)$. The substrate ($z < 0$) has permittivity ε_{sub} and the superstrate ($z > h$) has permittivity (1,0). When $0 \le z \le h$ and $0 < z < f(x)$, then $\varepsilon(x,z) = \varepsilon_{sub}$. When $0 \le z \le h$ and $h > z > f(x)$, then $\varepsilon(x,z) = (1,0)$. To solve the diffraction problem, we must obtain the solutions to Maxwell's equations

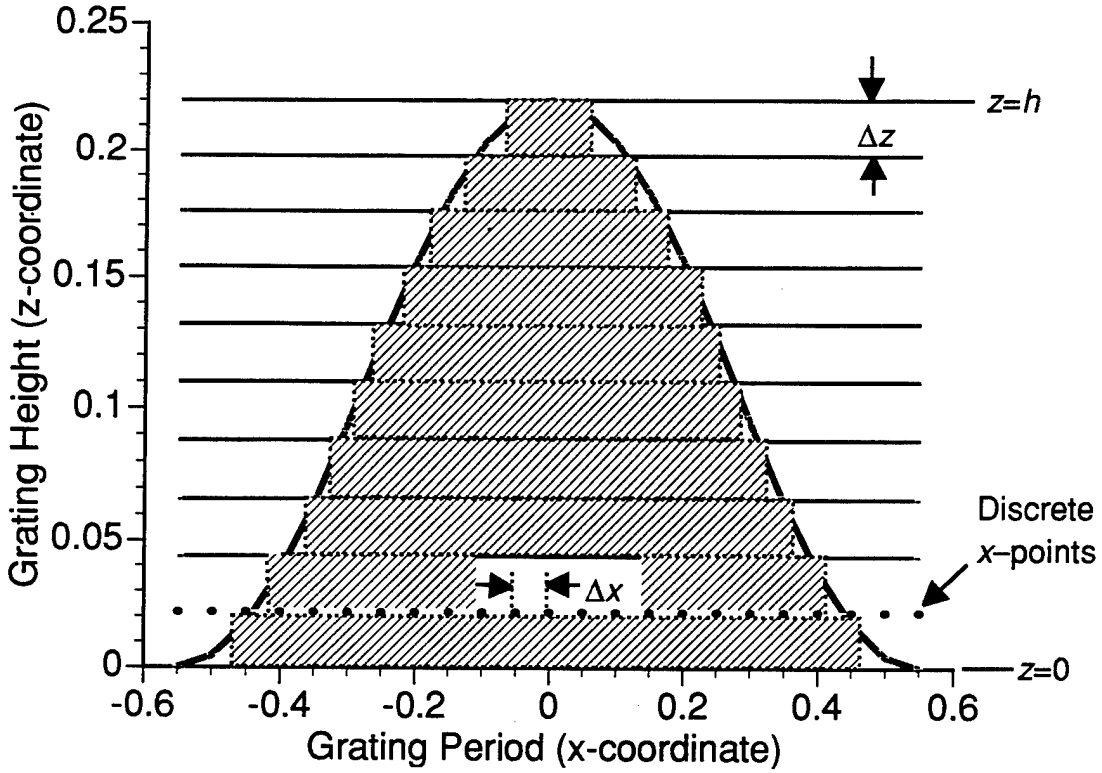

FIGURE 1. Schematic of Sinusoidal Grating Profile and Associated Nomenclature. The finite difference increments are Δx and Δz. A row of $n_x = 23$ digitized x-points is shown explicitly at $z = 0.022$ micrometers. There are $n_z = 10$ divisions of height h that yields for this example $\Delta z = 0.04\lambda = 0.022$ micrometers ($\lambda = 0.55$ micrometers). The shaded regions within the profile region show the actual profile shape based on the number of layers n_z since the permittivity $\varepsilon(x,z)$ is independent of z within each Δz layer.

throughout the profile region. To do this, we digitize the x-coordinate over period d into n_x discrete x values where each point is separated by $\Delta x = d/n_x$. We also discretize the z-coordinate into n_z values over height h where each point is separated by $\Delta z = h/n_z$. Maxwell's equations are now approximated with finite difference expressions:

$\nabla \times \mathbf{E}(x,z) = i(\omega/c)\mathbf{B}(x,z)$:

$$\frac{E_x(x,z+\Delta z) - E_x(x,z)}{\Delta z} = \frac{i\omega}{c} B_y(x,z)$$

$$+\frac{ic}{\omega(\Delta x)^2}\left\{\frac{B_y(x+\Delta x,z) - B_y(x,z)}{\varepsilon(x+\Delta x/2,z)} + \frac{B_y(x-\Delta x,z) - B_y(x,z)}{\varepsilon(x-\Delta x/2,z)}\right\} \quad (1a)$$

$$\frac{E_y(x,z+\Delta z) - E_y(x,z)}{\Delta z} = -\frac{i\omega}{c} B_x(x,z+\Delta z) \quad (1b)$$

$\nabla \times \mathbf{B}(x,z) = -i(\omega/c)\varepsilon(x)\mathbf{E}(x,z)$:

$$\frac{B_x(x,z+\Delta z) - B_x(x,z)}{\Delta z} = -\frac{i\omega}{c}\varepsilon(x,z)E_y(x,z)$$

$$+\frac{ic}{\omega(\Delta x)^2}\left\{2E_y(x,z) - E_y(x+\Delta x,z) - E_y(x-\Delta x,z)\right\} \quad (1c)$$

$$\frac{B_y(x,z+\Delta z) - B_y(x,z)}{\Delta z} = \frac{i\omega}{c}\varepsilon(x,z+\Delta z)E_x(x,z+\Delta z) \quad (1d)$$

In Equation 1, x and z are each a discrete coordinate in the set of n_x and n_z points. These equations, which apply to the profile region, are valid from $z = 0$ to $z = h$. For numerical purposes, we truncate the problem so that the integer index n_x ranges from $-N \rightarrow N$ and this means that when all x-points are included, Equation 1 represents $4(2N+1)$ equations for a given discrete z-value. If we include all $2N + 1$ x-points, Equation 1 may be arranged into a matrix equation having the form

$$\mathbf{r}_1\begin{pmatrix} E_x(\mathbf{X},z) \\ E_y(\mathbf{X},z) \\ E_x(\mathbf{X},z+\Delta z) \\ E_y(\mathbf{X},z+\Delta z) \end{pmatrix} = \mathbf{r}_2\begin{pmatrix} B_x(\mathbf{X},z) \\ B_y(\mathbf{X},z) \\ B_x(\mathbf{X},z+\Delta z) \\ B_y(\mathbf{X},z+\Delta z) \end{pmatrix} \quad (2)$$

where $\mathbf{r}_1$ and $\mathbf{r}_2$ are square matrices obtained from Equation 1 and $\mathbf{X}$ represents the set of n_x discrete x-points. The columns containing the x and y-components of E and B are column vectors where each of the E and B components have $2N+1$ elements and each element denotes a different x-coordinate. Defining a matrix $\mathbf{r} = \mathbf{r}_1^{-1}\mathbf{r}_2$ and abbreviating the column vectors with *tilde* notation as

$$\tilde{\mathbf{E}} = \begin{pmatrix} E_x \\ E_y \end{pmatrix} \text{ and } \tilde{\mathbf{B}} = \begin{pmatrix} B_x \\ B_y \end{pmatrix} \tag{3}$$

yields Equation 2 as

$$\begin{pmatrix} \tilde{\mathbf{E}}(\mathbf{X},z) \\ \tilde{\mathbf{E}}(\mathbf{X},z+\Delta z) \end{pmatrix} = \mathbf{r}(\Delta z) \begin{pmatrix} \tilde{\mathbf{B}}(\mathbf{X},z) \\ \tilde{\mathbf{B}}(\mathbf{X},z+\Delta z) \end{pmatrix} \tag{4}$$

This equation defines the $\mathbf{r}$ matrix for the layer bounded by $z \rightarrow z+\Delta z$ and needs to be calculated for each of the n_z layers. In constructing the $\mathbf{r}$ matrix, certain terms of Equations 1a and 1c require special attention. We note that for extreme x-values within a period, some field terms with arguments $x \pm \Delta x$ will fall outside the dimension of one period. These terms are "wrapped around" by using periodic boundary conditions (Bloch theorem). As described in detail in References 2 through 5, the fields at the $z = 0$ and $z = h$ planes may be related by a global relationship as

$$\begin{pmatrix} \tilde{\mathbf{E}}(\mathbf{X},0) \\ \tilde{\mathbf{E}}(\mathbf{X},h) \end{pmatrix} = \mathbf{R}(h) \begin{pmatrix} \tilde{\mathbf{B}}(\mathbf{X},0) \\ \tilde{\mathbf{B}}(\mathbf{X},h) \end{pmatrix} \tag{5}$$

where the square matrix $\mathbf{R}(h)$ is obtained by a recursive algorithm involving the $\mathbf{r}$ matrices for each of the n_z layers. Equation 5 is described in real-space, and it is convenient at this time to transform to Fourier space by means of the square matrix $\mathbf{F}(\mathbf{K},\mathbf{X})$ where

$$\mathbf{F}(\mathbf{K},\mathbf{X}) \begin{pmatrix} \tilde{\mathbf{E}}(\mathbf{X},0) \\ \tilde{\mathbf{E}}(\mathbf{X},h) \end{pmatrix} = \begin{pmatrix} \tilde{\mathbf{E}}(\mathbf{K},0) \\ \tilde{\mathbf{E}}(\mathbf{K},h) \end{pmatrix} \tag{6}$$

and similarly for the magnetic field. The vector $\mathbf{K}$ denotes the set of wave vectors in Fourier space analogous to the set $\mathbf{X}$ of x-coordinates in real space. We apply this $\mathbf{F}$ matrix to Equation 5 that yields

$$\begin{pmatrix} \tilde{\mathbf{E}}(\mathbf{K},0) \\ \tilde{\mathbf{E}}(\mathbf{K},h) \end{pmatrix} = \overline{\mathbf{R}}(h) \begin{pmatrix} \tilde{\mathbf{B}}(\mathbf{K},0) \\ \tilde{\mathbf{B}}(\mathbf{K},h) \end{pmatrix} \tag{7}$$

where the matrix $\overline{\mathbf{R}}(h) = \mathbf{F}\mathbf{R}(h)\mathbf{F}^{-1}$. Since the $z = 0$ and $z = h$ planes define the boundaries of the profile region adjoining the substrate and superstrate, respectively, we may match boundary conditions at these boundaries with the respective fields in the substrate and superstrate. At the substrate boundary, the boundary conditions may be written as $\tilde{\mathbf{E}}(\mathbf{K},0) = \tilde{\mathbf{E}}^t(\mathbf{K},0)$ and $\tilde{\mathbf{B}}(\mathbf{K},0) = \tilde{\mathbf{B}}^t(\mathbf{K},0)$ where the superscript t refers to the transmitted field region (substrate). At the superstrate boundary, the boundary conditions are $\tilde{\mathbf{E}}(\mathbf{K},h) = \tilde{\mathbf{E}}^{inc}(\mathbf{K},h) + \tilde{\mathbf{E}}^r(\mathbf{K},h)$ and $\tilde{\mathbf{B}}(\mathbf{K},h) = \tilde{\mathbf{B}}^{inc}(\mathbf{K},h) + \tilde{\mathbf{B}}^r(\mathbf{K},h)$ where the superscripts *inc* and r refer to the incident field and reflected field region (superstrate), respectively. Using these boundary conditions in Equation 7 yields

$$\begin{pmatrix} \tilde{\mathbf{E}}^t(\mathbf{K},0) \\ \tilde{\mathbf{E}}^{inc}(\mathbf{K},h) + \tilde{\mathbf{E}}^r(\mathbf{K},h) \end{pmatrix} = \overline{\mathbf{R}}(h) \begin{pmatrix} \tilde{\mathbf{B}}^t(\mathbf{K},0) \\ \tilde{\mathbf{B}}^{inc}(\mathbf{K},h) + \tilde{\mathbf{B}}^r(\mathbf{K},h) \end{pmatrix} \tag{8}$$

While transformation to Fourier space is convenient for diffraction calculations, it is also important since, in the homogeneous superstrate and substrate regions, a relation between **E** and **B** can be written as

$$\tilde{\mathbf{B}}^j(\mathbf{K},z) = \mathbf{Z}^j \tilde{\mathbf{E}}^j(\mathbf{K},z)$$

where $j = r$ or t. The form of the **Z** is given in References 2 through 4. With this relationship, we may finally write the end result as

$$\begin{pmatrix} \mathbf{I} - \overline{\mathbf{R}}_{11}\mathbf{Z}^t & -\overline{\mathbf{R}}_{12}\mathbf{Z}^r \\ -\overline{\mathbf{R}}_{21}\mathbf{Z}^t & \mathbf{I} - \overline{\mathbf{R}}_{22}\mathbf{Z}^r \end{pmatrix} \begin{pmatrix} \tilde{\mathbf{E}}^t(\mathbf{K},0) \\ \tilde{\mathbf{E}}^r(\mathbf{K},h) \end{pmatrix} = \begin{pmatrix} \mathbf{0} & \mathbf{R}_{12} \\ -\mathbf{I} & \mathbf{R}_{22} \end{pmatrix} \begin{pmatrix} \tilde{\mathbf{E}}^{inc}(\mathbf{K},h) \\ \tilde{\mathbf{B}}^{inc}(\mathbf{K},h) \end{pmatrix} \tag{9}$$

where the square matrix $\overline{\mathbf{R}}$ has been split into four quadrants each denoted by $\overline{\mathbf{R}}_{mn}$ with the appropriate m and n values. This matrix equation may be solved by standard means to calculate the transmitted $\mathbf{E}^t$ and reflected $\mathbf{E}^r$ fields.

NUMERICAL RESULTS

We assume a plane wave of wavelength λ = 0.55 micrometers is incident on the sinusoidal grating shown in Figure 1, where the incident polarization may be perpendicular or parallel to the grooves. The grating profile is given by $f(x) = h[1+\cos(2\pi x/d)]/2$. The gold substrate material has permittivity $\varepsilon_{sub} = (-5.28, 1.48)$ at λ = 0.55 micrometers. The numerical results are given for polarization parallel to the plane of incidence (perpendicular to the grooves). The numerical parameters used include $n_x = 83$ x-points which is the same as the number of diffracted orders and this yields $\Delta x = 0.0241\lambda$ = 0.0136 micrometers. We let $\Delta z = 0.1\Delta x$ which yields $n_z = 165$.

In Figure 2 we compare the present calculation method with the methods described in References 2 through 4. The input parameters n_x and n_z for the respective method are

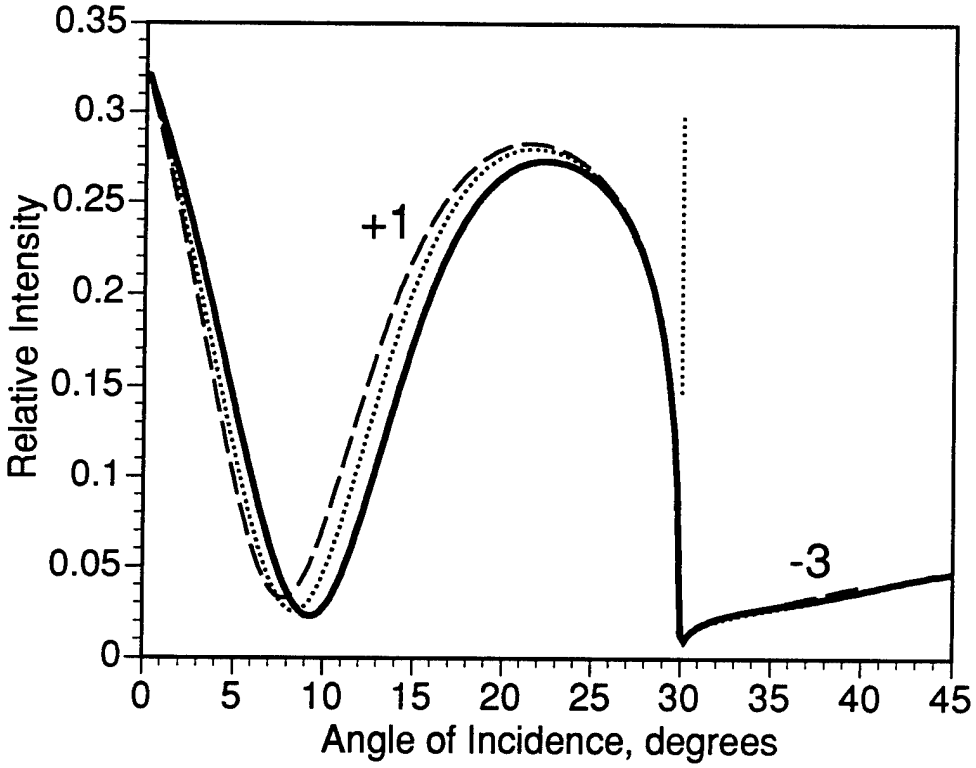

FIGURE 2. Comparison of Diffraction Intensity Versus Angle of Incidence For Three Methods of Calculation. The solid line is for the present numerical integration method. The dotted line is for the k-space method described in Reference 2. The dash line is from the real-space method described in References 3 and 4. The curves to the left and right of the vertical dotted line are for the +1 and -3 order, respectively. It is seen that the three methods are in close agreement.

shown in References 2 through 4, but the grating design and material parameters are the same as used here. It is seen that the three methods agree quite well.

Figure 3 compares the Depine (Reference 1) data with the present numerical integration method. There is considerable disagreement and the reason is not clear. In Depine's paper, he shows some numerical data that is based on a rigorous integral equation method and these data agree quite well with his approximate impedance boundary condition approach.

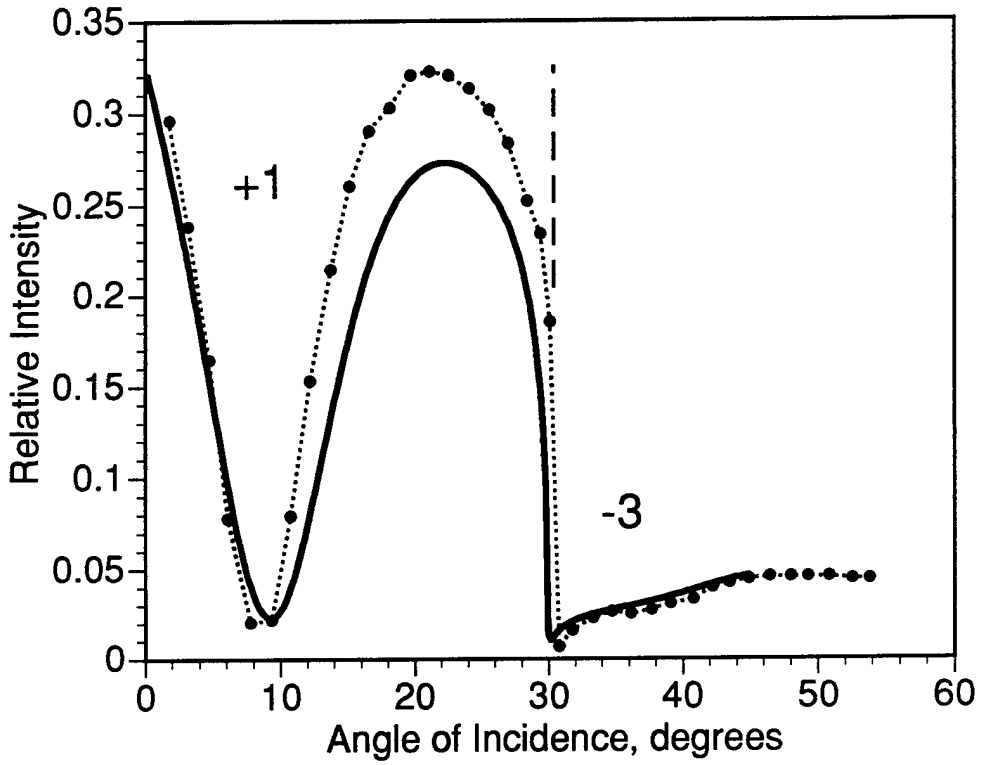

FIGURE 3. Diffraction Intensity Versus Angle of Incidence. These data compare the Depine results (dotted line with solid circles) with the present numerical integration method (solid). The vertical dash line separates the +1 and -3 diffracted orders. It is seen that there is moderate disagreement.

CONCLUSIONS

We have described a method of calculating grating diffraction that has the advantage of not requiring calculation of eigenvectors and eigenvalues. A disadvantage is that the numerical integration through the profile (z-direction) requires that the increment $\Delta z << \lambda$.

The method is versatile in that different grating profiles are simple to incorporate and extension to multilayered grating structures is possible in analogy with References 2 and 3.

The numerical results for the numerical example chosen here show agreement of the present method with two prior methods. Differences between these three methods, which are evident in Figure 2, may be decreased by varying discretization (numerical) parameters which can affect accuracy. The present method, and hence all three methods, are in moderate disagreement with Depine (Figure 7 contained in Reference 1). The reason for disagreement is left to future study.

ACKNOWLEDGMENTS

This work was supported by the Naval Air Warfare Center Weapons Division, China Lake Core S&T discretionary funding for fiscal year 1996 and by a grant of HPC time from the DOD HPC Center, U. S. Army Corps of Engineers Waterways Experiment Station (Cray Research C-916 and Y-MP).

REFERENCES

1. R. A. Depine. "Perfectly Conducting Diffraction Grating Formalisms Extended to Good Conductors Via the Surface Impedance Boundary Condition," *Appl. Opt.*, Vol. 26 (1987), pp. 2348-54. See Figure 7 of this work.

2. J. M. Elson and P. Tran. "Dispersion in Photonic Media and Diffraction From Gratings: A Different Modal Expansion for the **R**-Matrix Propagation Technique," *J. Opt. Soc. Am. A*, Vol. 12 (1995), pp. 1765-71.

3. J. M. Elson and P. Tran. "A Coupled Mode Calculation With the **R**-Matrix Propagator for the Dispersion of Surface Waves on a Truncated Photonic Crystal," *Phys. Rev.* B, Vol. 54 (1996), pp. 1711-15.

4. Naval Air Warfare Center Weapons Division. *A Real-Space, Modal Expansion Method With the **R**-Matrix Propagator to Calculate Grating Diffraction*, by J. M. Elson and P. Tran. China Lake, Calif., NAWCWPNS, September 1996. (NAWCWPNS TP 8318, publication UNCLASSIFIED.)

5. J. M. Elson and P. Tran. "Band Structure and Transmission of Photonic Media: a Real-Space Finite Difference Calculation With the **R**-Matrix Propagator," *NATO ASI Series E: Applied Sciences*, Vol. 315, ed. by Costas Soukoulis. Kluwer Academic Publishers. Pp. 341–54.

INITIAL DISTRIBUTION

1 Commander in Chief, U. S. Pacific Fleet, Pearl Harbor (Code 325)
1 Naval War College, Newport
1 Headquarters, 497 IG/INT, Falls Church (OUWG Chairman)
2 Defense Technical Information Center, Fort Belvoir
1 Center for Naval Analyses, Alexandria, VA

ON-SITE DISTRIBUTION

1 Code 400000D
1 Code 4B0000D
20 Code 4B1200D, Elson
1 Code 4B4000D, Chesnut
4 Code 4BL000D (3 plus Archives copy)